12th International Symposium on Turbulence and Shear Flow Phenomena (TSFP12)
Osaka, Japan (Online), July 19-22, 2022

STUDY OF BYPASS TRANSITION IN DENSE-GAS BOUNDARY LAYERS

Aurélien Bienner
DynFluid Laboratory
Arts et Metiers Institut of Technology
151 Bd. de l'Hopital, Paris (75013), France
aurelien.bienner@ensam.eu

Xavier Gloerfelt
DynFluid Laboratory
Arts et Metiers Institut of Technology
151 Bd. de l'Hopital, Paris (75013), France
xavier.gloerfelt@ensam.eu

Paola Cinnella
Jean Le Rond D'Alembert Institute
Sorbonne University
4 place Jussieu, Paris (75005), France
paola.cinnella@sorbonne-universite.fr

Leander Hake
Department of Mechanical Engineering
Muenster University of Applied Sciences
Stegerwaldstr. 39, Steinfurt (48565), Germany
leander.hake@fh-muenster.de

Stefan aus der Wiesche
Department of Mechanical Engineering
Muenster University of Applied Sciences
Stegerwaldstr. 39, Steinfurt (48565), Germany
wiesche@fh-muenster.de

Steffen Strehle
Microsystems Technology Group
Technische Universität Ilmenau
Max-Planck-Ring 12, Ilmenau (98693), Germany
steffen.strehle@tu-ilmenau.de

ABSTRACT

In a joint experimental/numerical effort to study the losses associated with freestream turbulence (FST) boundary-layer transition on turbine blades in organic Rankine cycles, we present the first large-eddy simulations of FST transition for the dense gas Novec^{TM}649 at high subsonic condition. Due to the small dimensions of the experimental apparatus, the boundary layer will experience relatively large-scale incoming disturbances. The results for conditions similar to the well-known T3A benchmark case are compared to cases with an integral length-scale of FST multiplied by ten with a high and low turbulence intensity. The size of the Klebanoff streaks, forerunners of the appearence of turbulent spots, is doubled and a relatively rapid onset of turbulence is observed even with the low level of turbulence. The effect of the dense gas relies essentially on its high heat capacity so that, even at high subsonic speeds, the transitional and turbulent states remains close to those observed in the incompressible regime.

INTRODUCTION

Organic Rankine cycle (ORC) power systems have become a popular technology for waste-heat recovery and environmentally-friendly power generation but relatively little is known regarding the impact of real-gas effects on loss mechanisms in ORC turbine expanders, which make use of molecularly complex organic fluids. In order to provide a deeper understanding of these loss mechanisms, a new experimental facility has been built at University of Muenster, which consists in a continuously running pressurized closed-loop wind tunnel using Novec^{TM}649, an environmentally friendly working fluid, in the high subsonic speed range. To further increase ORC turbine efficiencies, a better comprehension of free-stream turbulence (FST) transition, the principal mechanism of laminar-turbulent transition for turbine blades, in dense gases needs to be achieved. That is why the present study focuses on large-eddy simulations (LES) of FST transition for zero-pressure-gradient flat-plate boundary layers (ZPGFPBL) of Novec^{TM}649. As part of a Franco-German collaboration, a joint experimental and numerical study is undertaken. The experiments will be conducted in 2022 in the CLOWT wind tunnel (Reinker *et al.*, 2016) at the University of Muenster. Boundary layer (BL) measurements will be carried out on a sharp leading-edge silicon flat plate 2.5 mm thick, 6 cm long and 5 cm wide. The operating conditions for Novec^{TM}649 are given in table 1, corresponding to a Mach number M=0.9. Contrary to most FST experiments (Fransson & Shahinfar, 2020), the use of grid turbulence ahead of the flat plate is not directly possible due to the choking above M=0.5. Instead, the flow will be disturbed close to the leading edge using either electrical or sound mode excitation. Moreover, a FST transition with 2% of turbulence intensity, obtained by removing the multi-screen system, is planned. The very thin BL, which constitutes a considerable challenge for the measurements, will experience large-scale incoming turbulent structures. Miniaturized hot films will be inserted in the silicon wafer to follow the evolution of the friction at the wall.

To characterize the disturbances ahead of the plate, preliminary experiments of the decay of grid-generated homogeneous isotropic turbulence (HIT) for Novec^{TM}649 are conducted in the CLOWT facility. Hot-wire measurements at low speeds with a grid mesh size of 4 mm indicate a turbulence with an integral length scale $L_{11} \sim 3$ mm and a turbulence intensity $T_u \sim 2.8$ %. This corresponds to large disturbances and to a very high Reynolds number based on L_{11} ($Re_{L_{11}} \approx 9 \times 10^5$) at the chosen operating conditions, to be compared for instance

with the T3A case (Roach & Brierley, 1992), reproduced by numerous numerical simulations using $Re_{L_{11}}$ of the order of 1500. The aim of the present study is thus to investigate the role of large-scale disturbances on bypass transition for various T_u with the dense gas Novec^{TM}649 at M=0.9.

Table 1. Thermodynamic and aerodynamic conditions.

U_∞	c_∞	p_∞	T_∞	ρ_∞	μ_∞
[m/s]	[m/s]	[bars]	[°C]	[kg/m^3]	[μPa.s]
76.2	84.7	4	100	48.5	12.84

The influence of the FST characteristics on transition has been investigated experimentally and numerically for the ZPGFPBL configuration in the incompressible regime. Roach & Brierley (1992) observed in their experiments that, for the zero pressure gradient, the transition occurred earlier as T_u is increased. In the experiments of Jonas *et al.* (2000) at $T_u = 3\%$, it was found that the final stage of transition was advanced by FST with large scales whereas the extent of the transition region shortens with decreasing length scales. Brandt *et al.* (2004) reported that in their numerical simulations, for a fixed T_u, larger values of the integral length scale promotes earlier transition and noted that the spanwise scale of the streaks was only slightly affected by the FST scales, at least for $Re_{L_{11}}$ between 750 and 2250. More recently, Fransson & Shahinfar (2020) obtained experimentally two behaviours depending on the FST intensity: for low T_u ($\leq 2.45\%$), the transition was moved forward as L_{11} increased whereas the opposite was obtained with larger values of T_u ($\geq 2.8\%$).

A preliminary study of modal transition of a Novec^{TM}649 boundary-layer flow has been carried out (Bienner *et al.*, 2022) by introducing a pair of oblique modes. A reference direct numerical simulation (DNS) database for turbulent BL of Novec^{TM}649 has been generated and has enabled the validation of the implicit LES strategy retained in this paper, notably the resolution in wall units and the use of an implicit time advancement scheme. Based on these results, the present paper starts by recalling briefly the high-order numerical methods and the generation of synthetic turbulence at the inlet. Then, the LES results for various Tu and integral scales are presented and the transition patterns, specifically the generation of Klebanoff streaks, are analysed.

NUMERICAL METHODS AND SET-UP

Flow Solver MUSICAA

An in-house finite-difference code is used to solve the compressible Navier-Stokes equations. The inviscid fluxes are discretized by means of 10th-order standard centred differences whereas 4th-order is used for viscous fluxes. The scheme is supplemented with a 10th-order selective filtering to eliminate grid-to-grid unresolved oscillations and provide a selective regularization of subgrid-scales. A four-stage Runge-Kutta algorithm is used for time integration and a fourth-order implicit residual smooting (IRS4) method (Cinnella & Content, 2016) is implemented to enlarge the stability and allow the use of larger timesteps. Adiabatic no-slip conditions are applied at the wall, and non-reflecting Tam & Dong's conditions are imposed at the inlet, top and outflow boundaries. A sponge zone combining grid stretching and a Laplacian filter is added at the oulet. Periodicity is enforced in the spanwise direction. Concerning the fluid, the Novec^{TM}649 is modeled with the Peng-Robinson-Stryjek-Vera equation of state (Stryjek & Vera, 1986) and the Chung-Lee-Starling model (Chung *et al.*, 1988) for the transport properties. The MUSICAA solver has already been used in previous studies of wall-bounded flows of a dense gas (PP11): compressible channel flows (Sciacovelli *et al.*, 2017), supersonic boundary layers (Sciacovelli *et al.*, 2019), ...

Generation of Freestream Synthetic Turbulence

To generate incoming freestream turbulence, we use a synthetic velocity field, based on Random Fourier Modes (RFM) (Gloerfelt & Le Garrec, 2008). The homogeneous isotropic turbulent field is generated as the sum of N independent RFM:

$$\mathbf{u}'_{in}(\mathbf{x},t) = \sum_{n=1}^{N} \hat{u}_n \cos(\mathbf{k}_n.(\mathbf{x}-\overline{\mathbf{u}}t) + \omega_n t + \psi_n)\mathbf{a}_n \qquad (1)$$

Their amplitude is prescribed as $\hat{u}_n = \sqrt{2E(k_n)\Delta k_n}$, where $k_n = |\mathbf{k}_n|$ is the wavenumber discretized using the logarithmic distribution $\Delta k_n = (\ln k_{max} - \ln k_{min})/(N-1)$, with k_{min} and k_{max} the minimum and maximum mode wavenumbers, respectively. We use here a von Kármán spectrum with Saffman viscous dissipation function and a bottleneck correction:

$$E(k) = 1.453 \frac{(u'_{rms})^2 k^4/k_e^5}{\exp(17/6\log(1+(k/k_e)^2)} \times \exp\left(-1.5c_K(k\eta)^2\right) \times \left[(1+0.522\left(\frac{1}{\pi}\arctan(10\log_{10}(k\eta)+12.58)+\frac{1}{2}\right)\right] \qquad (2)$$

with $k_e = 0.747/L_{11}$, $c_K = 1.613$ and η the Kolmogorov viscous scale. In Eq.(1), ψ_n, $\mathbf{k}_n/k_n$, $\mathbf{a}_n$ are a random variables with given probability density functions. An unfrozen turbulent field is obtained by incorporating the convection velocity $\overline{\mathbf{u}}$ and the pulsation ω_n, accounting for the temporal evolution of the perturbations. In the present turbulent simulation, $N = 100$ and ω_n is deduced from Kolmogorov's theory, $\omega_n = \varepsilon^{1/3}k_n^{2/3}$, where ε is the the dissipation rate. The stochastic velocity field $\mathbf{u}'_{in}$ is entered using the Tam & Dong's inlet boundary condition (Gloerfelt & Le Garrec, 2008) and windowed by a van Driest type damping function to mimick the exponential damping of continuous Orr-Sommerfeld modes in the boundary layer. We use the function proposed by Pinto & Lodato (2019), defined as:

$$\sigma_{damp}(y) = (1 - e^{-y/(0.137\times h)})^{1000} \qquad (3)$$

where h corresponds to the height where the coefficient is equal to 0.5 and needs to be tuned by the user. This parameter has been shown to influence the transition location (Pinto & Lodato, 2019), as discussed later.

Simulation set-up

We select operating conditions representative of the future experimental campaign in CLOWT facility (see table 1) corresponding to a flow of Novec^{TM}649 at Mach 0.9 in relatively dilute conditions. The fundamental derivative of gas

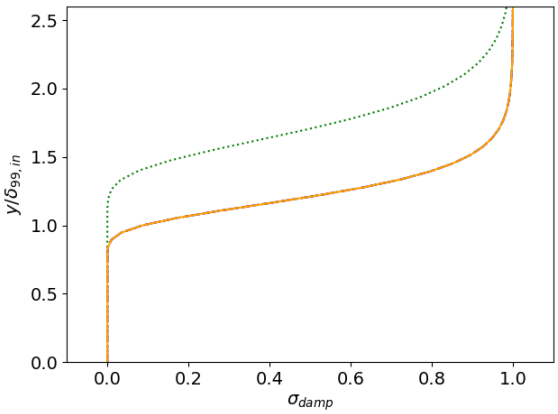

Figure 1. Damping coefficient applied close to the wall. The cases B, C and D are superposed.

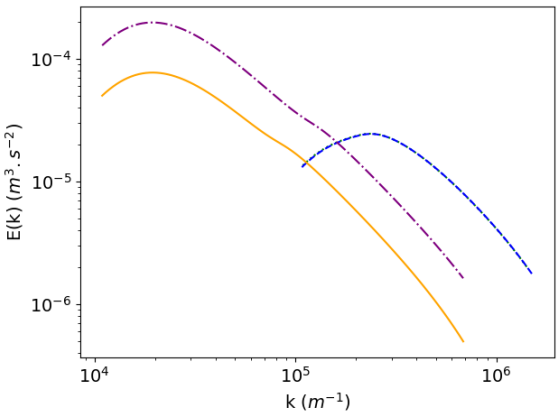

Figure 2. Initial kinetic energy spectra of inlet HIT. Cases A and B are superposed

dynamics has a value below 1 so that the flow occurs in the so called dense-gas thermodynamic region, as used in ORC applications. The flow properties are kept dimensional in the following since they are representative of the CLOWT experiments. The timestep is fixed to $\Delta t = 1.67 \times 10^{-9}$ s, which corresponds to a CFL of 4. In order to validate our numerical strategy, a first simulation, referred to as case A hereafter, is conducted to mimic the incompressible T3A experiment (Roach & Brierley, 1992). The Reynolds number at the inlet is taken as $Re_{x,in} = 10^4$, which corresponds to a boundary layer thickness $\delta_{99,in} = 1.73 \times 10^{-6}$ m. The injection height, defined by Eq.(3), is set to $h = 1.71\delta_{99,in}$. In case B, keeping the same FST characteristics as in case A (see table 2), the only changed parameter is h that is reduced to $1.21\delta_{99,in}$. This injection height is then kept fixed and two other LES simulations (C and D) are carried out with an integral length scale $L_{11,in}$ 10 times greater and with two different turbulence intensities T_u. The size of large-scale incoming disturbances is then more representative of the ones which will be encountered in CLOWT experiments at Mach 0.9.

Table 2. FST characteristics for the LES simulations.

Name	$Re_{L_{11,in}}$	$T_{u,in}$ (%)	$h/\delta_{99,in}$	Legend
A	1728	3.9	1.71	
B	1728	3.9	1.21	
C	17280	4	1.21	
D	17280	2.5	1.21	

The computational grid resolution needs to comply with two major constraints. The first one concerns the resolution of the near-wall boundary layer flow. As mentionned in the introduction, a first study of Novec^{TM}649 BL transition by oblique modes has been conducted (Bienner *et al.*, 2022). This provides us a target resolution to achieve in the turbulent BL of $\Delta x^+ \times \Delta y_w^+ \times \Delta z^+ \sim 30 \times 1.0 \times 11$. The second constraint is the resolution of the freestream disturbances. As the synthetic turbulence is injected by a limited number of modes, which needs to remain as small as possible in order to avoid excessive computational overcost, the k_{min} and k_{max} of the inlet energy spectra Eq.(1) are selected as follows. Since the peak kinetic energy is localised around L_{11}, k_{min} is determined so that the crossflow dimensions L_y and L_z are greater than $9L_{11,in}$. We then choose $k_{max} \geq 64k_{min}$, which yields a maximal value for the grid spacings to accurately resolve every injected modes, based on the numerical scheme used. The resolution of the simulations is given in table 3 and the inlet spectra are plotted in figure 2. For cases A and B, the major constraint is given by the freestream turbulence characteristics whereas, for cases C and D, as the integral length scale is relatively large, the near-wall resolution constraint is more restrictive.

Table 3. Computational grid properties for FST simulations.

Case	Points $(N_x \times N_y \times N_z)$	Resolution $\Delta x^+ \times \Delta y_w^+ \times \Delta z^+$	$R_{\theta,end}$
A	$1920 \times 204 \times 62$	$13 \times 1.1 \times 13$	1100
B	$1824 \times 280 \times 80$	$13 \times 1.0 \times 11$	2950
C	$1800 \times 480 \times 780$	$28 \times 0.9 \times 10$	2200
D	$1800 \times 480 \times 780$	$27 \times 0.9 \times 10$	2050

INFLUENCE OF LARGE-SCALE DISTURBANCES ON FST TRANSITION

As already pointed out, case A is carried out to mimic the T3A experiments (Roach & Brierley, 1992). The FST characteristics are determined thanks to preliminary simulations of spatially decaying HIT (not presented here), in order to match the FST evolution of the turbulence intensity in the T3A experiment, as recommended by Pinto & Lodato (2019), who also used synthetic turbulence for this benchmark case. The selected values are given in table 2. When L_{11} is increased or decreased, the decay slope of the FST evolution is decreased or increased, respectively. For case A, the integral length scale $L_{11,in} = 6 \times 10^{-6}$ m corresponds to $Re_{L_{11,in}} = 1728$, and the inlet T_u is 3.9%. These values are coherent with the ones in Pinto & Lodato (2019) ($Re_{L_{11}} = 1950$, $T_u = 3.5\%$) and comprised in the range investigated by Brandt *et al.* (2004), where $Re_{L_{11}}$ is

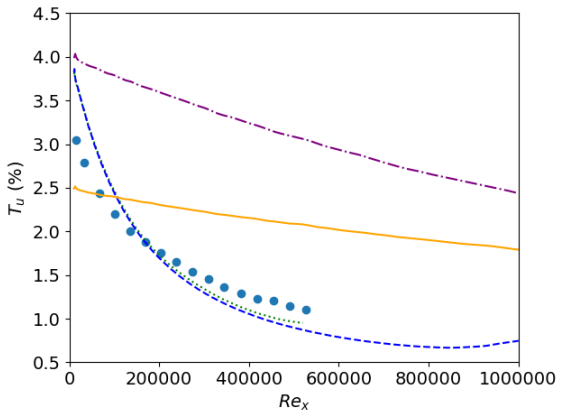

Figure 3. Evolution of the freestream turbulence intensity.

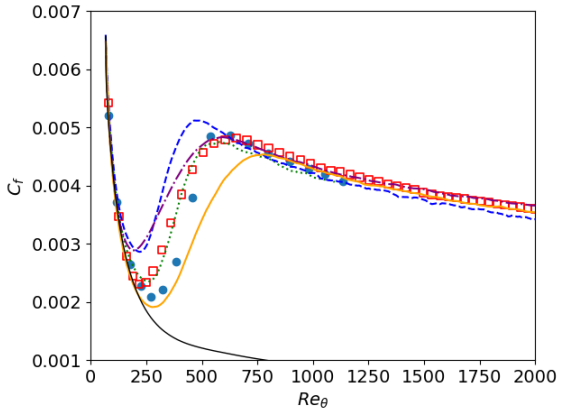

Figure 4. Evolution of the friction coefficient.

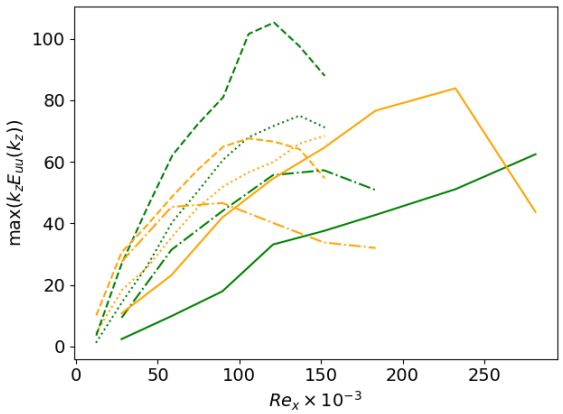

Figure 5. Streamwise evolution of the spectra $k_z E_{uu}(k_z)$ maximum for $\lambda_{z,1}$ and $\lambda_{z,2}$. Linestyles as in tab. 2.

varied between 750 and 2250. The freestream turbulence evolution is plotted in figure 3 along with the T3A experimental data (•). The decay rate for case A is in reasonable agreement with the reference. The distributions of the friction coefficient C_f for all cases are plotted in figure 4, along with T3A experimental data (•), the laminar Blasius correlation $0.664/\sqrt{Re_x}$ (——), and the DNS of bypass transition of Wu & Moin (2009) (□). The injection height h of the inlet turbulence has been shown to be a sensitive parameter for the transition onset (Pinto & Lodato, 2019). The value $h = 1.71\delta_{99,in}$ used in case A yields a transition location in fair agreement with T3A. It is slightly higher than the one for which Pinto & Lodato (2019) better reproduced the T3A transition location ($h = 1.5\delta_{99,in}$) since their numerical methods are different. It is also worthy to note that the present C_f evolutions follow closely the ones obtained in the incompressible regime despite the present high subsonic Mach number of 0.9. As shown in Bienner *et al.* (2022), the high heat capacity of Novec^{TM}649 reduces drastically the friction heating at the wall so that no compressibility effects are observed on the velocity profiles. The mean streamwise velocity fluctuation profiles, scaled by the friction velocity u_τ, are plotted in figure 7 for the different cases and the experimental data. The profiles for case A are in good agreement with the experimental ones.

The second simulation (case B) is performed with the same FST conditions but with a lower injection height h (see figure 1). As there is no universal value for the injection height h, the choice is made here to inject FST just above the edge of the inlet BL at $1.21\delta_{99,in}$. As expected, the FST T_u decay for case B is seen to perfectly match the one of case A in figure 3 since their initial energy spectra are superposed in figure 2. The C_f evolution in figure 4 indicates that a reduced h promotes a faster transition, which can be beneficial numerically in term of the minimal streamwise extent to capture a fully turbulent state. This value of h has been chosen and kept constant for cases C and D to allow the investigation of the influence of large-scale disturbances on FST transition. The slope of the C_f rise is similar for the two injection heights in cases A and B but the value of $u'_{rms,max}$ in figure 7 is greater at the location $Re_x = 67 \times 10^3$ since the onset of transition is already reached at the following stations.

In order to observe the influence of a large L_{11} value of the incoming FST, the integral length scale is multiplied by a factor of ten in cases C and D, yielding a $Re_{L_{11}}$ of 17.28×10^3. For case C, the inlet turbulence intensity is kept close from the $T_{u,in}$ values of case A and B. As L_{11} is large, the FST decay is slow and its intensity remains high all along the computational domain as seen in figure 3. Compared to case B, the slope of the C_f rise in the transition region is smoother in figure 4 and, even if the transition onset occurs earlier, the end of the transition region is slightly shifted downstream. A similar trend has been observed in Fransson & Shahinfar (2020) for high turbulent intensity ($T_u \geq 2.8\%$). In case D, the T_u is reduced to 2.5% to approximatively match the T_u obtained for case B at the beginning of the transition region. The reduction of T_u in case D causes the transition to move further downstream, with a slope of C_f in the transition region slightly steeper with respect to case C. Moreover, because of the slow decay rate of FST in cases C and D, an enhancement, more pronounced for case C, of the turbulent BL skin friction is observed, with a C_f slighty higher than in case B. An instantaneous view of the streamwise velocity for case D is depicted in figure 8. The xy-slice clearly shows the large sizes of the energetic turbulent scales in the freestream compared to the BL thickness. The formation of the Klebanoff mode and the presence of turbulent spots are clearly revealed in the top view.

Close-up views near the inlet are proposed in figure 9 for the four cases, with the same dimensional streamwise and spanwise extents, and provide a first qualitative comparison of the Klebanoff modes. In cases A and B, we observe that the spanwise width and spacing of the streaks are very similar. The comparison between cases C and D is less obvious, even if it is clear that the scales associated with Klebanoff modes are very different between the cases A-B and the cases C-D. To get further insights into these differences, spanwise wavenumber

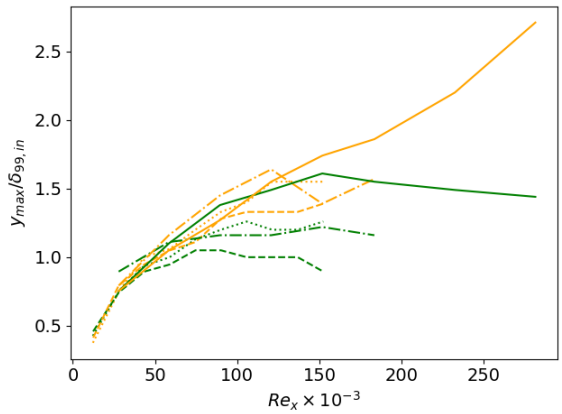

Figure 6. Streamwise evolution of the position of the spectra maximum for $\lambda_{z,1}$ and $\lambda_{z,2}$. Linestyles as in tab. 2.

premultiplied spectra $k_z E_{uu}$ of the streamwise velocity fluctuations at successive locations along the boundary layer have been realised. The spectra are averaged over at least 1500 time samples in case D and up to 3000 in case B, and the peaks in the crossflow plane λ_z-y indicate the emergence at a preferential height of several Klebanoff modes in the transition region. The evolution of the intensity and wall-normal location of the two main peaks are reported in figures 5 and 6, respectively. Mode 1, corresponding to the spanwise wavelength $\lambda_{z,1}$, dominates first and the harmonic mode 2, with wavelength $\lambda_{z,2} = \lambda_{z,1}/2$, takes over more or less rapidly proportionately to the length of the transitional region. The wavelengths of the selected modes are given in table 4. Their mean wall-normal height, plotted in 6, is determined by their size. The first growth phase is remarkably similar for all cases. The spanwise scales observed in the spectra are similar between cases C and D, whereas they differ by a factor of approximately 2 with respect to the case B, which is coherent with figure 9. More advanced statistics, based on streak identification (Nolan & Zaki, 2013), will be used to refine the present analysis.

Table 4. Values of $\lambda_{z,1}$ and $\lambda_{z,2}$.

Name	A	B	C	D
$\lambda_{z,1}/\delta_{99,in}$	9.6	9.6	18.0	18.0
$\lambda_{z,2}/\delta_{99,in}$	4.8	4.8	9.0	9.0

CONCLUSIONS AND FUTURE WORK

In the present study, we have investigated the bypass transition of a zero-pressure gradient flat-plate BL in a high subsonic organic vapor flow. At the chosen thermodynamic conditions, there is no peculiar non-ideal real gas effects. Due to the high specific heat of Novec^{TM}649, the friction heating at the wall is significantly reduced and the behaviour is close to the incompressible regime. Given the dimensions involved in the forthcoming experimental campaign in CLOWT facility, we are primarily interested by the influence of large-scale freestream turbulence on transition. The LES results show that the high increase of the integral length scale tends to delay transition and increase the spanwise scales of the Klebanoff streaks. For the large cases, the decrease of T_u moves the transition downstream. In the turbulent state, the FST slighty enhances the wall friction in presence of large scales, due to the weak decay rate of FST along the streamwise direction. We observed that the injection height at the inlet is a tunable parameter that influences the onset of transition. To get rid of that artefact, we will include the leading edge in the future simulations to observe the shear sheltering effect. By varying the curvature of the leading edge, we will be able to investigate the effect of a favorale pressure gradient. This will constitute the next step before tackling a blade configuration representative of ORC turbines.

ACKNOWLEDGEMENTS

This research has been funded by the Agence Nationale de la Recherche through the ANR-20-CE92-0019-02 project Regal-ORC. This work was granted access to the HPC resources of IDRIS and TGCC under the allocation A0092A01736 made by GENCI (Grand Equipement National de Calcul Intensif).

REFERENCES

Bienner, A., Gloerfelt, X. & Cinnella, P. 2022 Numerical study of boundary-layer transition in a high-subsonic organic vapor flow. *56th 3AF Conference* 28-30 March, Toulouse, France, FP108-AERO2022 .

Brandt, L., Schlatter, P. & Henningson, D.S. 2004 Transition in boundary layers subject to free-stream turbulence. *J. Fluid Mech.* **517**, 167–198.

Chung, T.H., Ajlan, M., Lee, L.L. & Starling, K.E. 1988 Generalized multiparameter correlation for nonpolar and polar fluid transport properties. *Industrial & Engineering Chemistry Research* **27** (4), 671–679.

Cinnella, P. & Content, C. 2016 High-order implicit residual smoothing time scheme for direct and large eddy simulations of compressible flows **326**, 1–29.

Fransson, J. & Shahinfar, S. 2020 On the effect of free-stream turbulence on boundary-layer transition. *J. Fluid Mech.* (899), A23.

Gloerfelt, X. & Le Garrec, T. 2008 Generation of inflow turbulence for aeroacoustic applications. *14th AIAA/CEAS AeroAcoustics Conference,* 5-7 May, Vancouver, Canada, AIAA Paper 2008-2926 .

Jonas, P., Mazur, O. & Uruba, V. 2000 On the receptivity of the by-pass transition to the length scale of the outer stream turbulence. *European Journal of Mechanics - B/Fluids* **19**, 707–722.

Nolan, K. P. & Zaki, T. A. 2013 Conditional sampling of transitional boundary layers in pressure gradients. *J. Fluid Mech.* **728**, 306–339.

Pinto, B. & Lodato, G. 2019 Synthetic freestream disturbance for the numerical reproduction of experimental zero-pressure-gradient bypass transition test cases. *Flow, Turbulence and Combustion* (103), 25–54.

Reinker, F., Hasselmann, K., aus der Wiesche, S. & Kenig, E.Y. 2016 Thermodynamics and fluid mechanics of a closed blade cascade wind tunnel for organic vapors. *ASME Journal of Engineering for Gas Turbines and Power* **138**, 052601–1–052601–8.

Roach, P. E. & Brierley, D. H. 1992 The influence of a turbulent free stream on zero pressure gradient transitional boundary layer development. part 1: testcases t3a and t3b.

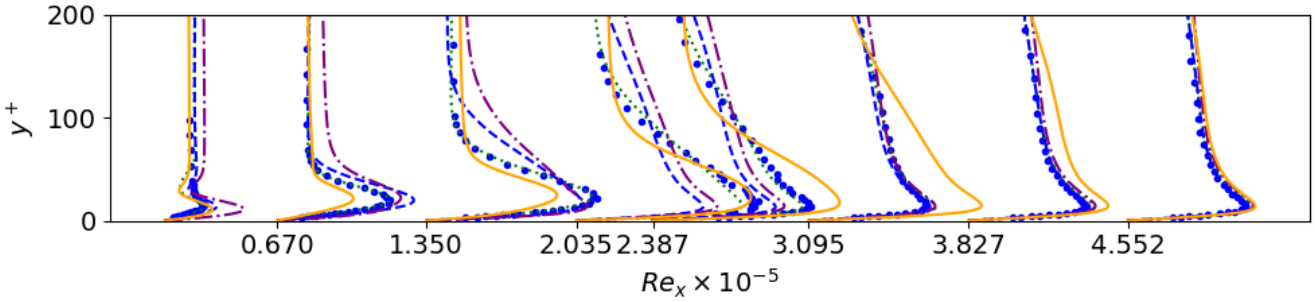

Figure 7. Scaled streamwise fluctuating velocity: $0.2*(u'_{rms}/u_\tau) + Re_x/10^5$.

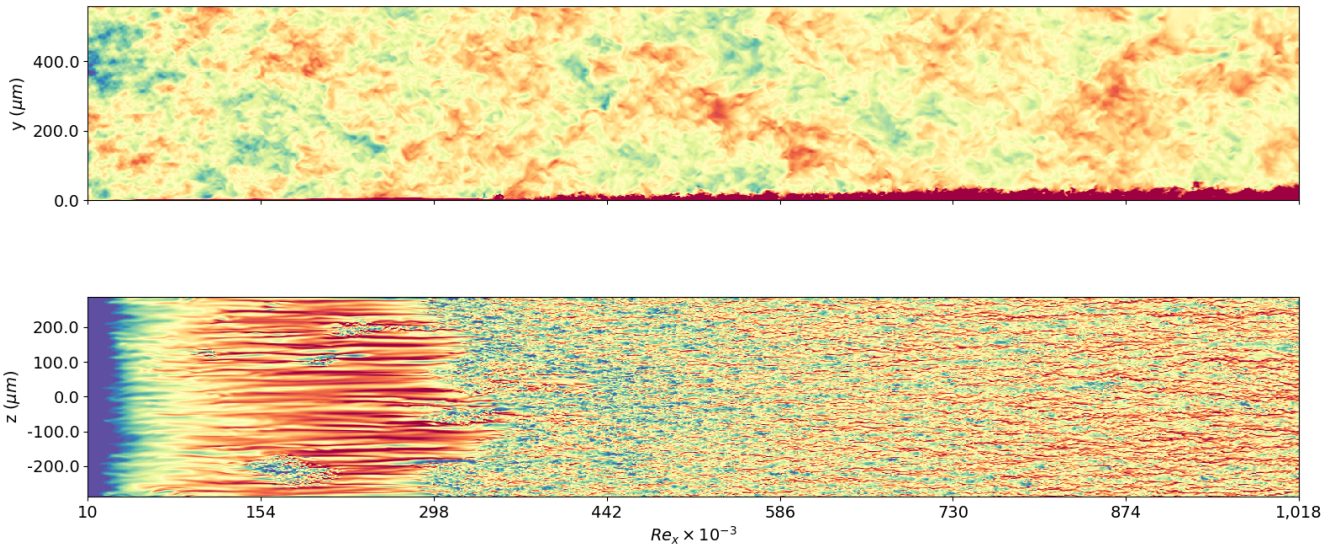

Figure 8. Instantaneous slice xy (top) at $z = 0$ and xz (bottom) at $y/\delta_{99,in} = 1.1$ for case D shown for the full domain. The values are plotted between $0.9U_\infty$ (red) and $1.1U_\infty$ (blue) at the top and $0.3U_\infty$ (red) and $0.9U_\infty$ (blue) at the bottom.

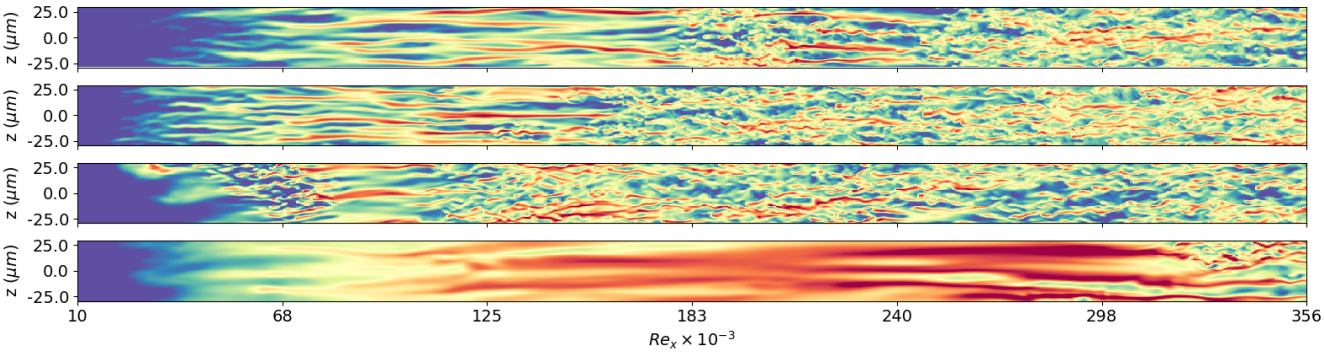

Figure 9. Instantaneous slice of plane normal to the wall at the location $y/\delta_{99,in} = 1.3$ for case A and $y/\delta_{99,in} = 1.1$ for case B, C and D. The values are plotted between $0.3U_\infty$ (red) and $0.9U_\infty$ (blue). From top to bottom: case A, B, C and D.

Numerical simulation of unsteady flows and transition to turbulence pp. 319–347.

Sciacovelli, L., Cinnella, P. & Gloerfelt, X. 2017 Direct numerical simulations of supersonic turbulent channel flows of dense gases. *J. Fluid Mech.* **821**, 153–199.

Sciacovelli, L., Gloerfelt, X., Cinnella, P. & Grasso, F. 2019 Numerical investigation of hypersonic boundary layers of perfect and dense gases. *Flow, Turbulence and Combustion* In redaction.

Stryjek, R. & Vera, J.H. 1986 PRSV: An improved Peng-Robinson equation of state for pure compounds and mixtures. *The Canadian Journal of Chemical Engineering* **64** (2), 323–333.

Wu, X. & Moin, P. 2009 Direct numerical simulation of turbulence in a nominally zero-pressure-gradient flat-plate boundary layer. *J. Fluid Mech.* **360**, 5–41.